

Supporting information for

## Single-crystal caged gold nanorods with tunable broadband plasmon resonances

**Wei Xiong,<sup>a,b,c</sup> Debabrata Sikdar,<sup>d</sup> Michael Walsh,<sup>e</sup> Kae Jye Si,<sup>b,c</sup> Yue Tang,<sup>b,c</sup> Yi Chen,<sup>b,c</sup> Romiza Mazid,<sup>b,c</sup> Matthew Weyland,<sup>e,f</sup> Ivan D. Rukhlenko,<sup>d</sup> Joanne Etheridge,<sup>e,f</sup> Malin Premaratne,<sup>d</sup> Xinyong Li,<sup>a</sup> and Wenlong Cheng<sup>\*b,c</sup>**

<sup>a</sup> Key Laboratory of Industrial Ecology and Environmental Engineering and State Key Laboratory of Fine Chemical, School of Environmental Sciences and Technology, Dalian University of Technology, Dalian 116024, China.

<sup>b</sup> Department of Chemical Engineering, Monash University, Clayton 3800, Victoria, Australia.

<sup>c</sup> The Melbourne Centre for Nanofabrication, 151 Wellington Road, Clayton 3168, Victoria, Australia.

<sup>d</sup> Advanced Computing and Simulation Laboratory (A $\chi$ L), Department of Electrical and Computer Systems Engineering, Monash University, Clayton 3800, Victoria, Australia.

<sup>e</sup> Department of Materials Engineering, Monash University, Victoria 3800, Australia.

<sup>f</sup> Monash Centre for Electron Microscopy, Monash University, Victoria 3800, Australia

\*Email: wenlong.cheng@monash.edu

## **Table of Contents**

**Section 1 Method**

**Section 2 Characterizations of CGNRs**

**Section 3 DDA Simulation of Broadband Resonances**

**Section 4 References**

## Section 1 Method

**Chemicals:** Gold (III) chloride trihydrate ( $\text{HAuCl}_4$ ), hexadecyltrimethylammonium bromide (CTAB), silver nitrate ( $\text{AgNO}_3$ ), sodium borohydride ( $\text{NaBH}_4$ ), L-ascorbic acid (AA), Cetyltrimethylammonium chloride (CTAC, 25 wt.% in  $\text{H}_2\text{O}$ ), and Polyvinylpyrrolidone (PVP) were obtained from Sigma Aldrich. All glassware and Teflon-coated magnetic stir bars were cleaned with aqua regia, followed by thorough rinsing with deionized water before drying in an oven at  $80^\circ\text{C}$

**Synthesis of Au nanorods:** The gold NRs with different length were prepared according to the well-established seed-mediated growth method.<sup>1</sup> A brownish-yellow seed solution was prepared by mixing CTAB (5.0 mL, 0.2 M) and  $\text{HAuCl}_4$  (5.0 mL, 0.5 mM) followed by adding ice-cold  $\text{NaBH}_4$  (0.6 mL, 0.01 M). The seed solution was aged at  $27^\circ\text{C}$  before seeding to growth solution. Then, CTAB (5 mL, 0.20 M) and  $\text{HAuCl}_4$  (5.0 mL, 1.0 mM) were added to 4 mM  $\text{AgNO}_3$  solution in sequence and with the addition of AA (0.08 mL, 0.08 M), the yellowish mixture became colorless and the growth solution was obtained. To grow NRs, 12  $\mu\text{L}$  of premade seed was added into the growth solution and aged at  $30^\circ\text{C}$  for two hours. The CTAB capped NRs were collected by centrifugation (7 000 rpm for 10 min) and washed with water twice. NRs with various lengths were synthesized by changing the volume of  $\text{AgNO}_3$  ranging from 50 to 200  $\mu\text{L}$ . The NRs with three different lengths were synthesized and named by NR-S, NR-M, and NR-L, corresponding to 50, 100 and 200 mL  $\text{AgNO}_3$  solutions, respectively.

**Synthesis of AuNR@AgNCs:** The AuNR@AgNCs were prepared according to the procedure reported previously.<sup>2</sup> The NR-L solution was centrifuged, followed by redispersion in an aqueous solution of CTAC to a total volume of 10 mL and kept for more than 12 h to ensure total replacement of CTAB by CTAC. This will lead to a faster nucleation and rapid growth of silver metal on gold nanorods as well as a more uniform shell formation.<sup>3</sup> The NR-L solution was then

kept at 65°C in oil bath and then AgNO<sub>3</sub> (850 μL, 10 mM) were added dropwisely, respectively and then followed by the addition of AA (100 mM). The volume was a half of the AgNO<sub>3</sub> solution used in each batch. The resultant solution was continually stirred at 65°C for 3 h. The CTAC capped AuNR@AgNCs were collected by centrifugation (7 000 rpm for 10 min) and washed with water twice. The same procedure was performed on NR-S and NR-M, except for the volume of AgNO<sub>3</sub> and AA added. For these, AgNO<sub>3</sub> (500 μL) was added to NR-S and AgNO<sub>3</sub> (600 μL) to NR-M, while the addition of AA was still a half of AgNO<sub>3</sub> added. Note that the silver shell thickness was highly dependent on the volume of AgNO<sub>3</sub> (10 mM) solution added. For NR-L, we deliberately set another three different volumes 550, 700, and 1000 μL 10 mM AgNO<sub>3</sub> solution, which gave AuNR@AgNCs with four different silver thicknesses.

**Synthesis of Caged Gold Nanorods:** The CGNRs were prepared via the galvanic replacement reaction by using AuNR@AgNCs as sacrificial templates, PVP as surfactant and CTAB as surfactant and complexing agent.<sup>4</sup> The AuNR@AgNCs prepared were centrifuged and redispersed in 2.5 mL deionized water, followed by the addition of CTAB (5 mL, 0.2 M) solution and PVP (2.5 mL, 2 wt%) solution sequentially. 1 mL of the resultant solution was mixed in a thermomixer at 90 °C for 2 minutes. Various volumes of HAuCl<sub>4</sub> (0.5 mM) were added immediately and mixed for another 10 minutes ranging from 5 μL to 400 μL. High temperature is maintained to ensure dissolution of AgCl generated during the reaction and epitaxial deposition of gold atoms on the silver nanocuboids surfaces. For the optical evolution of CGNRs during the galvanic replacement reaction, increasing volumes of HAuCl<sub>4</sub> precursor was added in drop by drop (10, 30, 50, 70, 90, 110, 120, 140, 160, 190, 210, 260, and 320 μL, respectively). The CGNRs were collected by centrifugation (6 500 rpm for 10 min) and washed with water twice.

**Structural and optical characterization:** Scanning electron microscopy (SEM) images of the nanostructures were taken with a field emission SEM (JEOL 7001 F). Absorption spectra were recorded using an Agilent 8453 UV–vis spectrometer. Transmission electron microscopy (TEM) images of the nanostructures were taken with Hitachi H7500 TEM. HAADF STEM was performed on a FEI Tecnai G2 F20 S-Twin FEG STEM, operating at 200 kV. STEM samples were prepared by dropping 5  $\mu$ L of the colloidal suspension onto a holey carbon TEM grid, followed by washing in pure ethanol before being allowed to dry in ambient conditions. Energy dispersive X-ray (EDX) maps of CGNRs were acquired on a JEOL 2100F FEG scanning transmission electron microscope (STEM) operating at 200kV, equipped with a JEOL 50mm<sup>2</sup> Si(Li) X-ray detector. EDX maps of CGNRs were recorded at x1.5M magnification, with a nominal probe size of 0.7 nm.

**Numerical Modelling:** To calculate the absorption spectra of the caged gold nanorods, we used the numerical simulation tool DDSCAT 7.2,<sup>5</sup> which is a discrete dipole approximation (DDA) method, implemented by Draine and Flatau.<sup>6</sup> This method allows us to estimate the absorption and scattering of incident electromagnetic radiation by any arbitrary-shaped nanoparticle, where the target can be represented as an array of polarizable points. We adopted this method because of its faster computing efficiency as compared to other numerical tools<sup>7</sup> and also the privilege with which we were able to describe the complex structure of CGNRs in a dipole array, specifying the location of the dipoles and the nature of material in each sub-volume of the structure, where a dipoles is centered. In each case of simulating the absorption spectra of, the nanocuboids describing structural evolution to a CGNR, an intact CGNR, and ruptured CGNRs, we considered inter-dipole spacing 'd' to be 1 nm; implying that the total number of dipoles 'N' increases with the size of the target geometry. Then the electric field  $\mathbf{E}_j$  at position  $j$  of a point dipole, with polarization given as  $\mathbf{P}_j = \alpha_j$

$\mathbf{E}_j$ , in the dipole array ( $j \in [1, N]$ ) can be calculated as sum of incident electric field  $\mathbf{E}_{inc,j}$  and field contributions coming from remaining  $N-1$  dipoles, given by<sup>5-6</sup>

$$\mathbf{E}_j = \mathbf{E}_{inc,j} - \sum_{k \neq j} \mathbf{A}_{jk} \mathbf{P}_k$$

where  $\mathbf{A}_{jk} \mathbf{P}_k$  is the electric field at location  $j$  arising from point dipoles at remaining locations in the structure. Upon solving these  $3N$  complex linear equations for the unknown polarizations  $\mathbf{P}_j$ , DDSCAT evaluates the absorption efficiency for an incident electric field of  $\mathbf{E}_0$ , using the following expression:<sup>5-6</sup>

$$Q_{abs} = \frac{C_{abs}}{\pi a_{eff}^2} = \frac{4k}{|E_0|^2 a_{eff}^2} \sum_{j=1}^N \left\{ \text{Im}[P_j (\alpha_j^{-1})^* P_j^*] - \frac{2}{3} k^3 |P_j|^2 \right\}$$

where  $a_{eff}$  is the effective radius of a sphere equal to the volume of the target nanocuboid. To consider for randomly oriented nanocuboids in this work, we computed absorption spectra for longitudinally and transversely polarised light and computed an averaged spectra with weights of 1/3 and 2/3 respectively. In each case the orientation averaging was getting numerically computed in DDSCAT based on the expression given as<sup>5-6</sup>

$$\langle Q_{abs} \rangle = \frac{1}{8\pi^2} \int_0^{2\pi} d\beta \int_0^{2\pi} d\phi Q_{abs}(\beta, \vartheta, \varphi)$$

where  $\beta$ ,  $\vartheta$ , and  $\varphi$  the angles representing the orientation of the target nanoparticle in DDSCAT tool's 'lab frame'.<sup>6</sup> Note that  $\vartheta$  is considered to be  $90^\circ$  in case of longitudinal polarization and  $0^\circ$  in case of transverse polarization.

## Section 2 Characterization of CGNRs

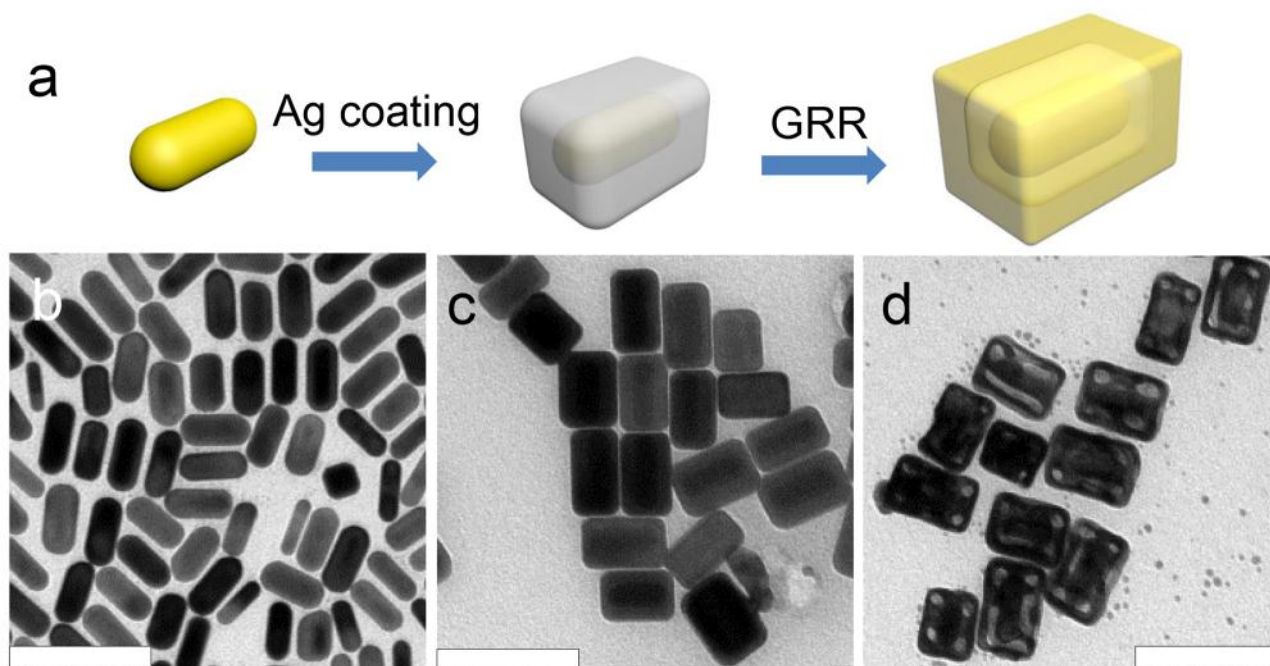


Fig. S1. (a) Scheme of synthesis of caged gold nanorods. Yellow and grey represent gold and silver, respectively. TEM images of NRs (b), AuNR@AgNCs (c) and CGNRs (d). Scale bar: 100 nm.

CGNRs were synthesized via a three-step protocol, namely (i) synthesis of gold nanorods, (ii) coating the gold nanorods with silver and (iii) galvanic replacement reaction of silver by gold to form cage. In details, capsule-like gold NRs are first synthesized, collected by centrifugation and then, redispersed in CTAC solution. Next, silver is coated onto gold nanorod surface, leading to the formation of gold NRs embedded into silver nanocuboids. AuNR@AgNCs are purified by centrifugation and mixed with a solution containing hexadecyltrimethylammonium bromide (CTAB) and polyvinylpyrrolidone (PVP). Finally, the mixture is heated up to 90°C, followed by addition of HAuCl<sub>4</sub> and then the CGNRs were synthesized.



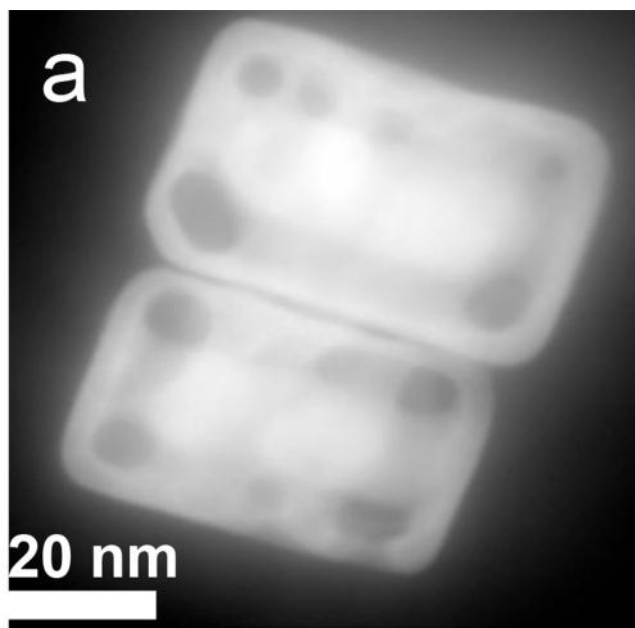


Fig. S2 HAADF STEM of two CGNRs for SAD in Fig. 1b



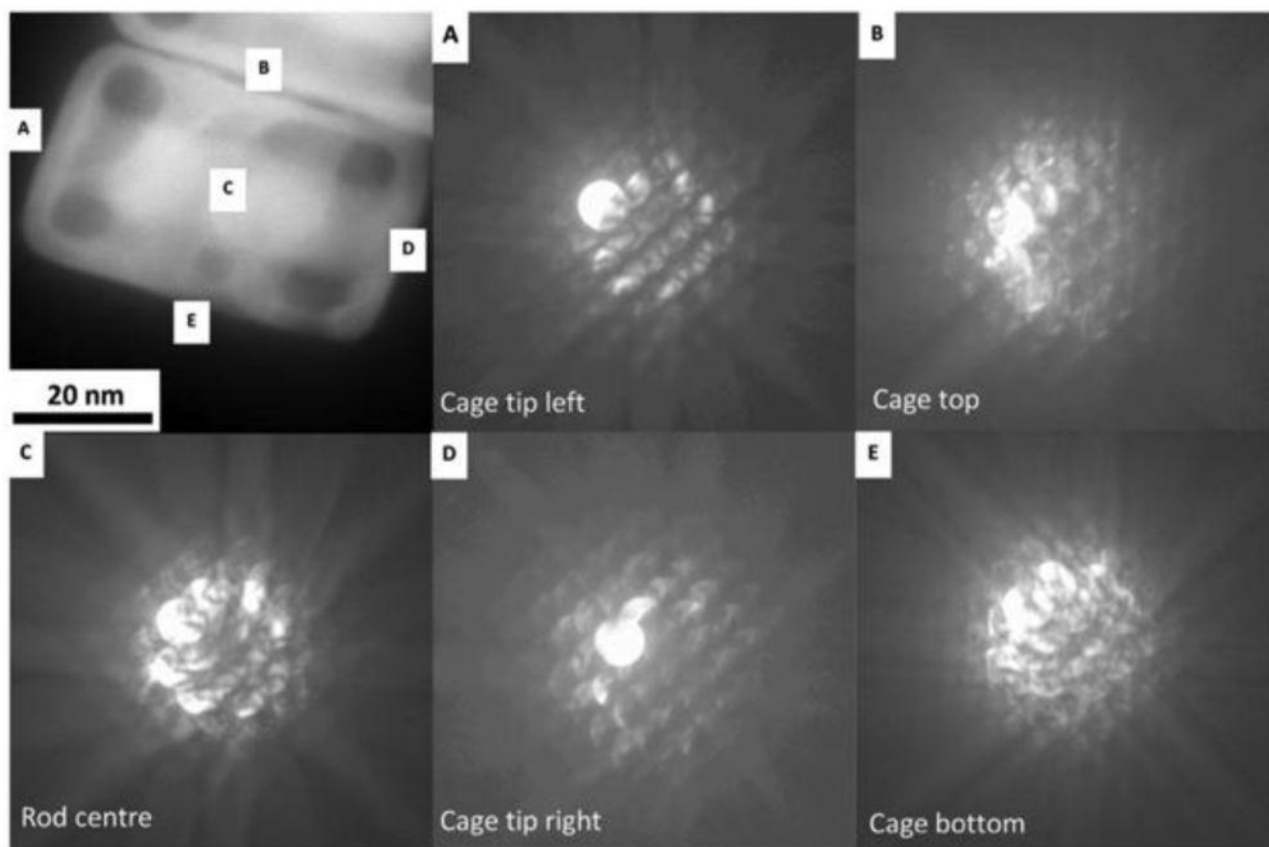


Fig. S3. HAADF STEM and CBED patterns from a CGNR. The CGNR was synthesized via the galvanic replacement reaction performed on AuNR@AgNC which was prepared by adding 850  $\mu\text{L}$   $\text{AgNO}_3$  solution to NS-L solution. Convergent beam electron diffraction was used to provide localized structural analysis of the CGNR's. For the caged nanorod shown, the sub-nm diameter electron probe was focused on various areas of the nanorod and cage, and the corresponding CBED pattern recorded. Such analysis of individual CGNRs, in this case close to the [001] orientation, confirmed that the NR and each side of its surrounding cage have the same crystal structure and orientation.

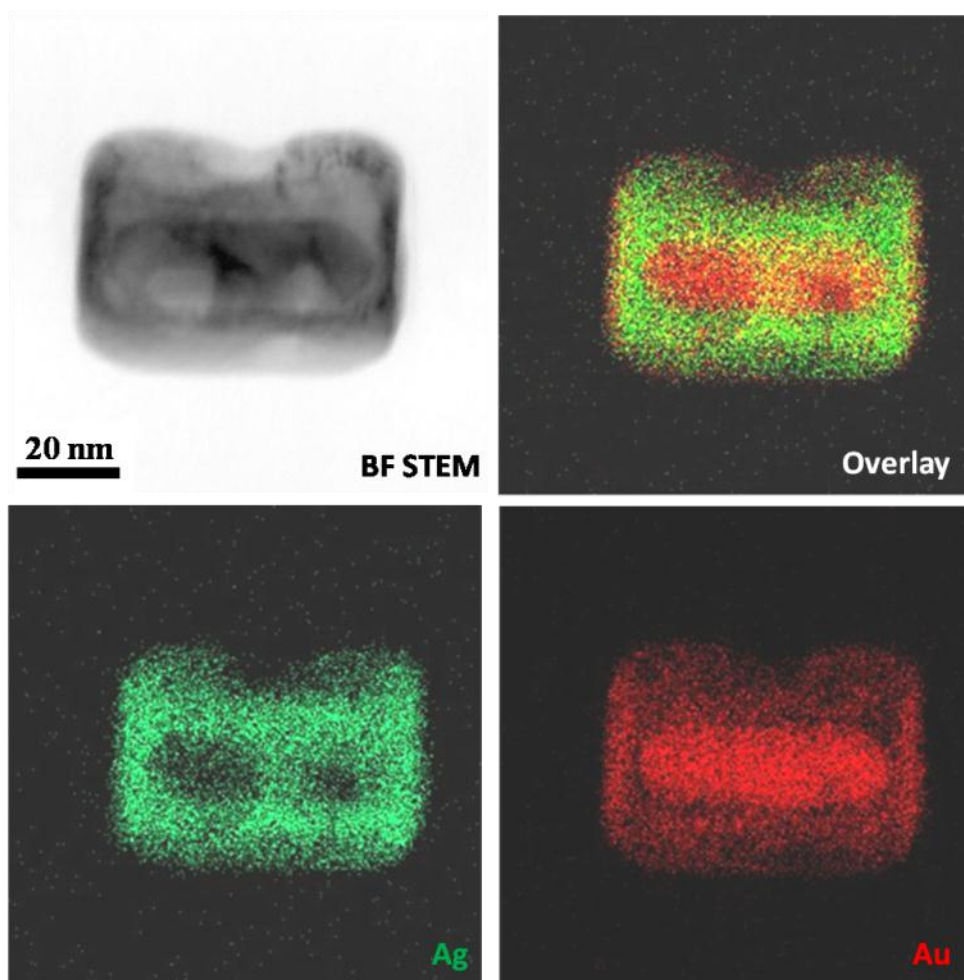
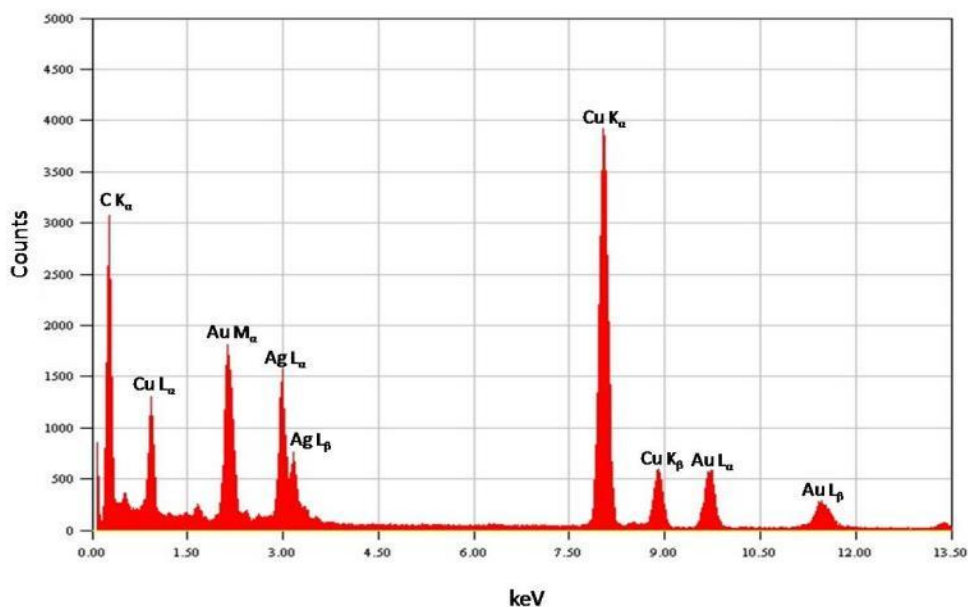


Fig. S4. EDX spectra and maps of a CGNR. Ag L and Au M lines were mapped using a dwell time of 0.2 msec over 56 sweeps. Copper and carbon peaks come from the Cu/C TEM support grid.

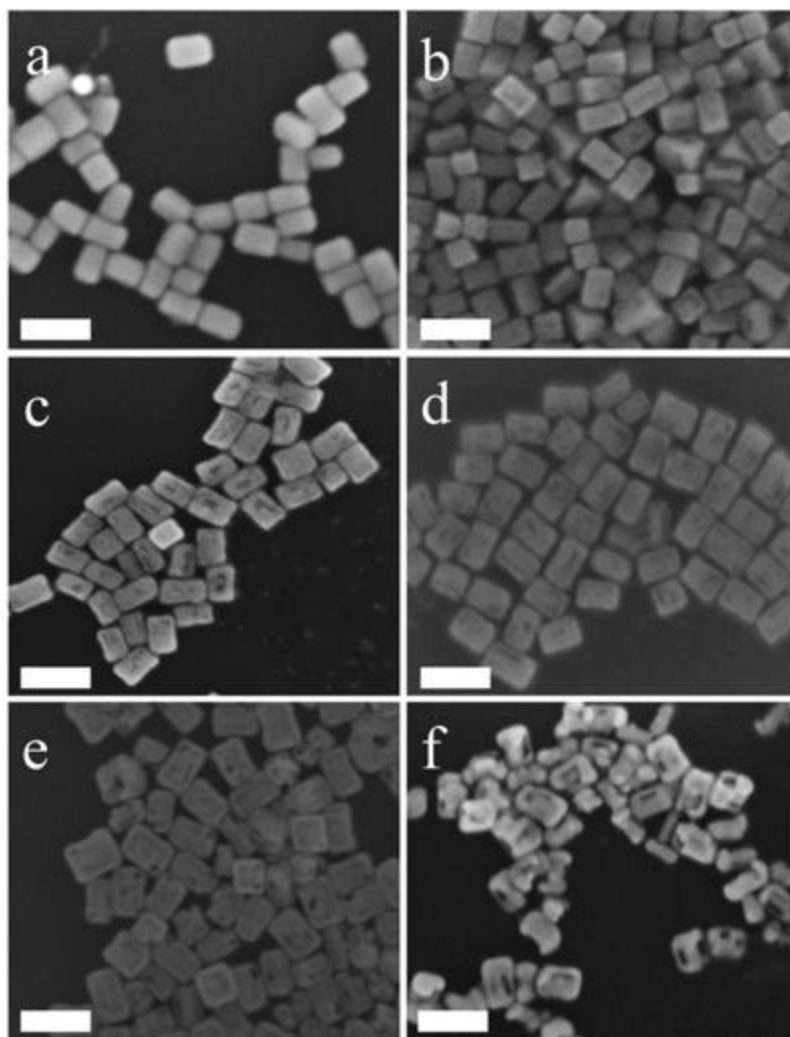


Fig. S5. (a) SEM of AuNR@AgNCs, (b)-(h) SEM of CGNRs synthesized by different volumes of 0.5mM HAuCl<sub>4</sub> precursor: 30, 80, 110, 160, 300  $\mu$ L. The AuNR@AgNCs were prepared by adding 850  $\mu$ L AgNO<sub>3</sub> solution to NS-L solution.

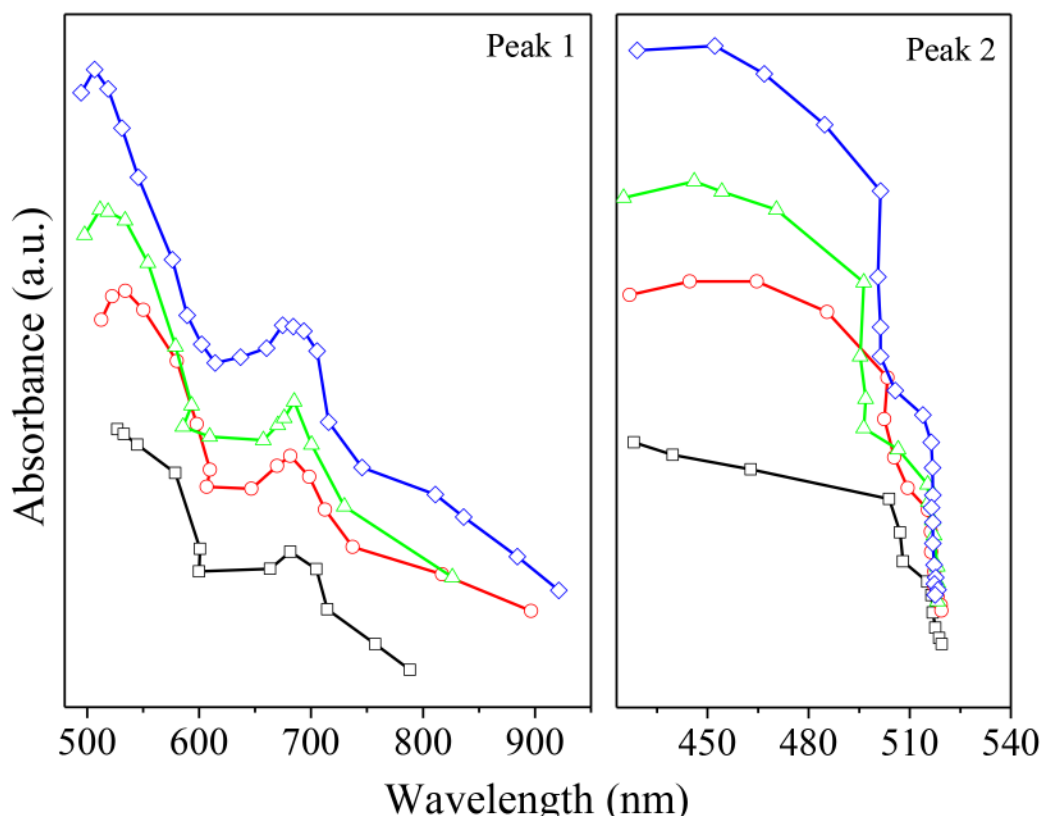


Fig. S6. Shifts of characteristic peaks 1 and 2 over the entire galvanic replacement reaction. The four batches of CGNRs were derived from AuNR@AgNCs which were prepared by adding 550  $\mu\text{L}$  (black), 700  $\mu\text{L}$  (red), 850  $\mu\text{L}$  (green) and 1000  $\mu\text{L}$  (blue)  $\text{AgNO}_3$  solution to NS-L solution, respectively. Note that all four batches showed the similar trend of peak shifting. Both peaks 1 and 2 redshift and broaden (Fig. 2c). Peak 2 shifts at a slower rate than peak 1, but decays in intensity more quickly. Peak 2 stops shifting at around 520 nm, but its intensity continually decreases with increasing amounts of  $\text{HAuCl}_4$  added. In contrast, peak 1 continues to redshift into the near-infrared region. In the intermediate stage, the intensity reaches a maximum, possibly indicating the formation of intact cuboid-shaped nanocages, free from pinholes or rupturing. Further GRR could de-alloy the cage, rupturing the cage walls and leading to the intensity decrease of peak.

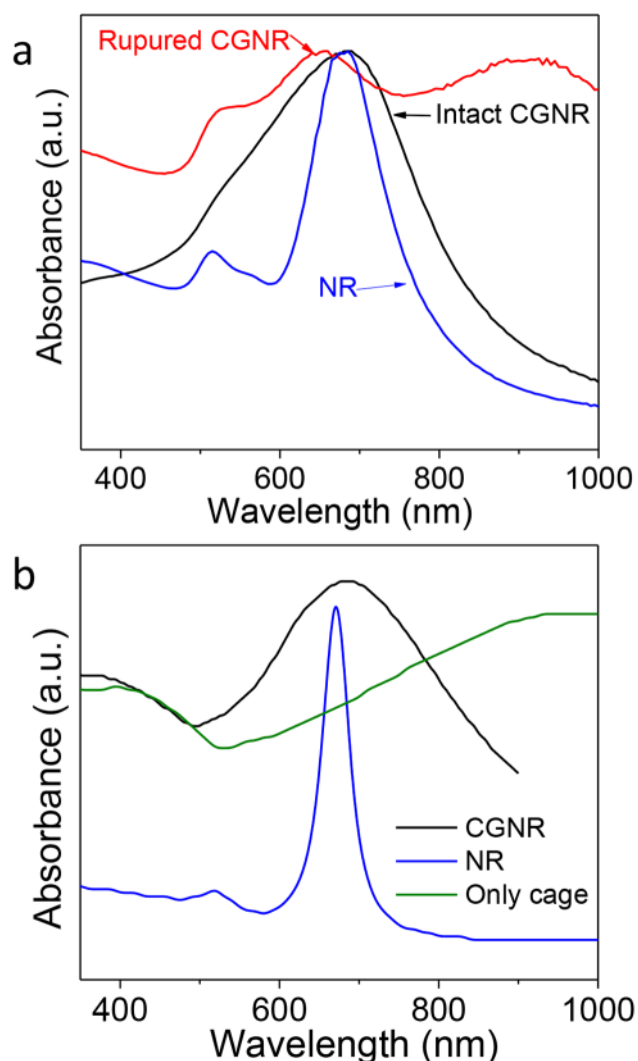


Fig. S7. (a) Experimental UV-vis spectra of intact CGNRs and ruptured CGNRs compared with original NRs; (b) Calculated absorbance spectra for a single intact CGNR, NR and nanocage only. The galvanic replacement reaction was performed on AuNR@AgNCs which were prepared by adding 1000  $\mu\text{L}$   $\text{AgNO}_3$  solution. 240  $\mu\text{L}$  0.5 mM  $\text{HAuCl}_4$  was used to titrate the AuNR@AgNCs solutions in order to obtain intact CGNRs while 400  $\mu\text{L}$   $\text{HAuCl}_4$  to ruptured CGNRs. Note that intact CGNRs exhibited two broadband surface plasmon resonance peaks, whereas ruptured CGNRs showed three resonance peaks due to exposure of NRs.

It is seen that the broadband plasmon resonance characteristic arises due to the caging effect, where the spectral features of the gold nanorod embedded inside gets screened by the resonance properties of the cage. Due to enhanced surface scattering of electrons in nano-cage walls, the SPR

peak of caged gold nanorod gets significantly broadened, which are shown in Fig. S7a (experiment) and S7b (simulation). The resonance feature of a ruptured gold nanorod (seen experimentally) shows that when the nanocage breaks, spectral features arising from both gold nanorod and gold cage (seen in simulation) can be separately identified. The resonance peak of an intact caged nanorod lies close to the longitudinal dipolar resonance peak of the individual gold nanorod, and exhibits significant spectral broadening.

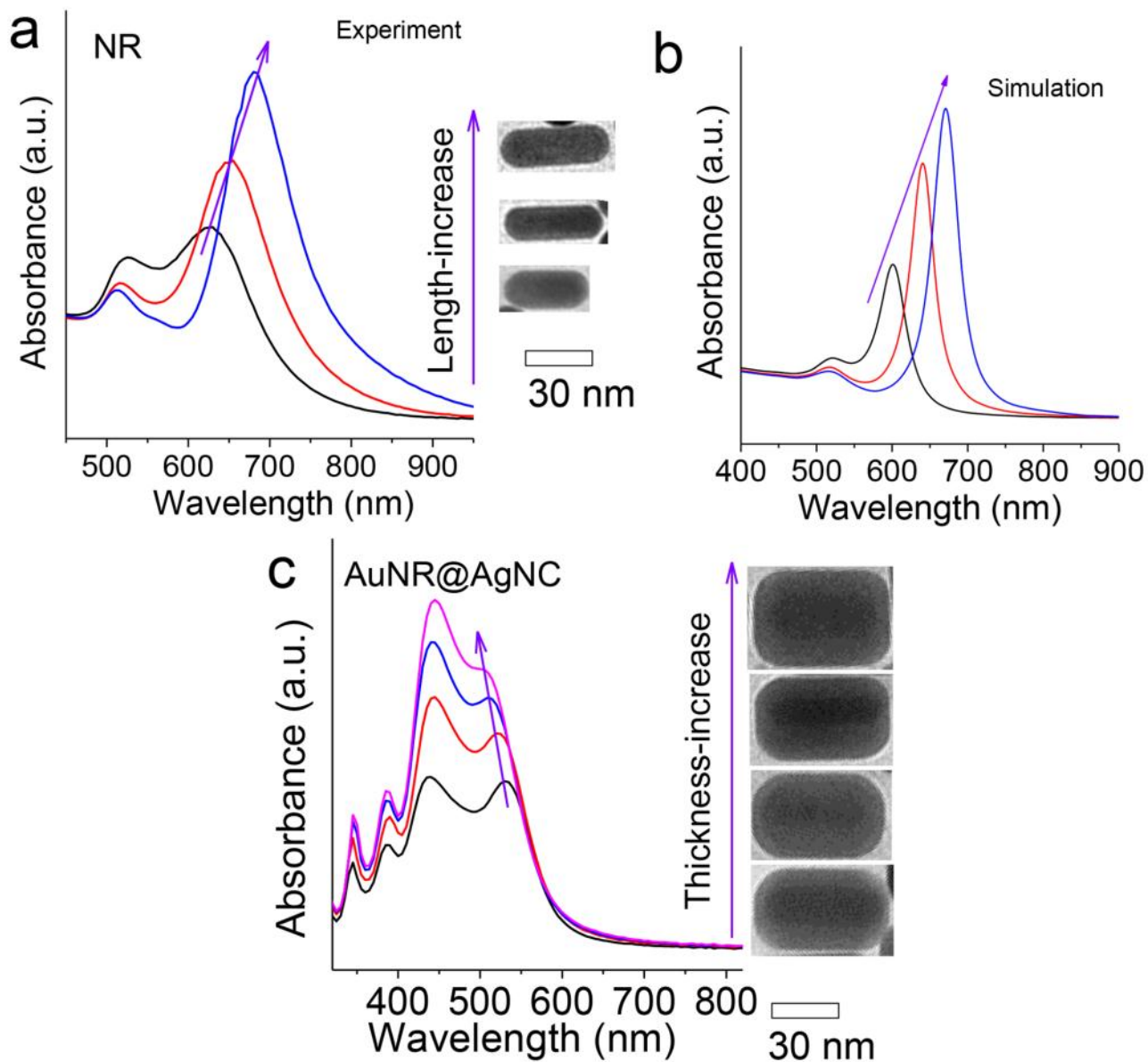


Fig. S8 (a) Experimental and (b) calculated UV-vis spectra of length-tunability of NRs; and (c) width-tunability of AuNR@AgNCs.

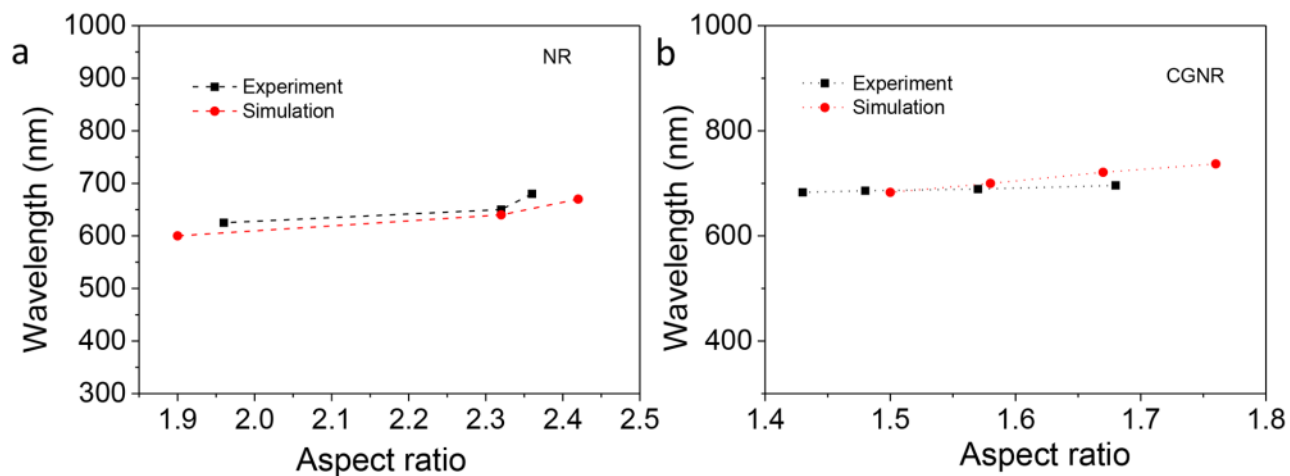


Fig. S9 Plot of plasmon peak wavelength vs. the aspect ratio of gold NRs (a) and CGNR (b): comparison of the experiment and simulation.

	$L_{NR}$	$W_{NR}$	$AR_{NR}$		$L_{CGNR}$	$W_{CGNR}$	$AR_{CGNR}$
	(nm)	(nm)	(nm)		(nm)	(nm)	(nm)
Experiment	40.1	20.5	1.96		60.4	42.3	1.43
	43.9	18.9	2.32		59.9	40.4	1.48
	46.1	19.5	2.36		59.0	37.6	1.57
					58.1	34.5	1.68
Simulation	40	21	1.90		60	40	1.50
	44	19	2.32		60	38	1.58
	46	19	2.42		60	36	1.67
					60	34	1.76



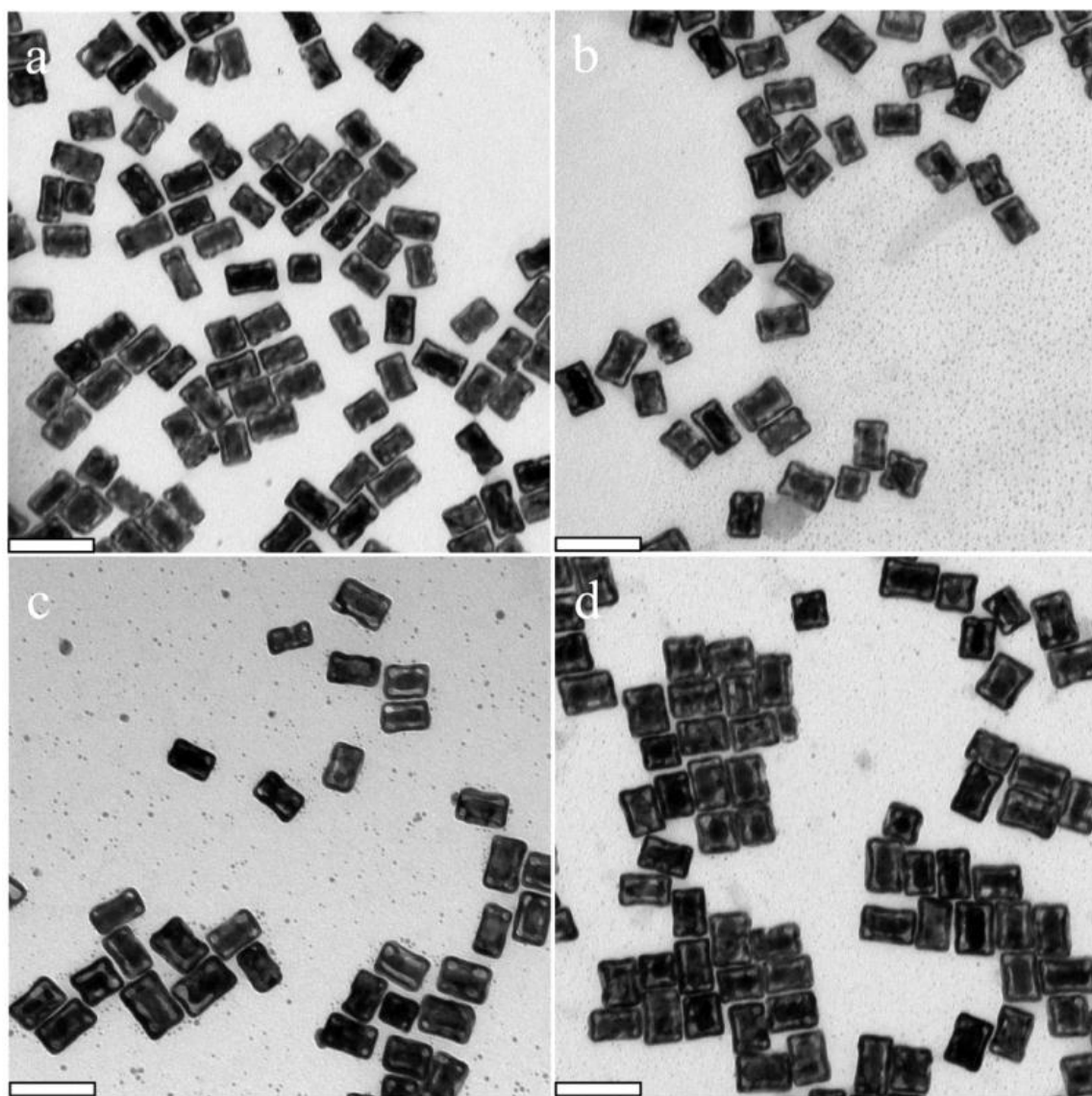


Fig. S10. TEM of intact CGNRs with different widths. The intact CGNRs were derived from AuNR@AgNCs which were prepared by adding 550  $\mu\text{L}$  (black), 700  $\mu\text{L}$  (red), 850  $\mu\text{L}$  (green) and 1000  $\mu\text{L}$  (blue)  $\text{AgNO}_3$  solution to NS-L solution respectively. Scale bar: 100 nm.

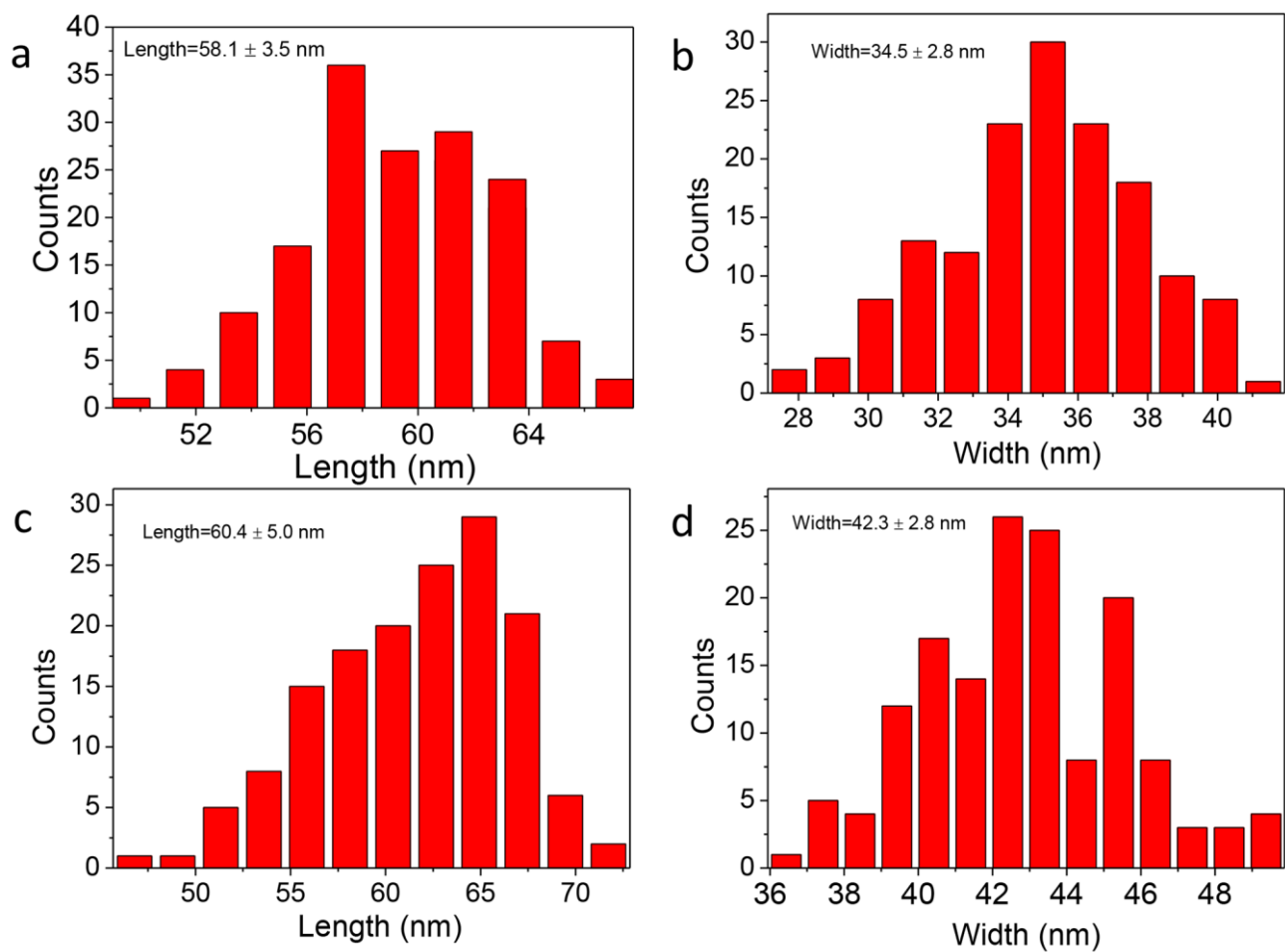


Fig. S11. Size distribution of CGNRs. (a)(b) length and width distribution of CGNRs whose TEM as shown in Fig. S10a and (c)(d) length and width distribution of CGNRs whose TEM as shown in Fig. S10d.

### Section 3 DDA Simulations of Broadband Resonances

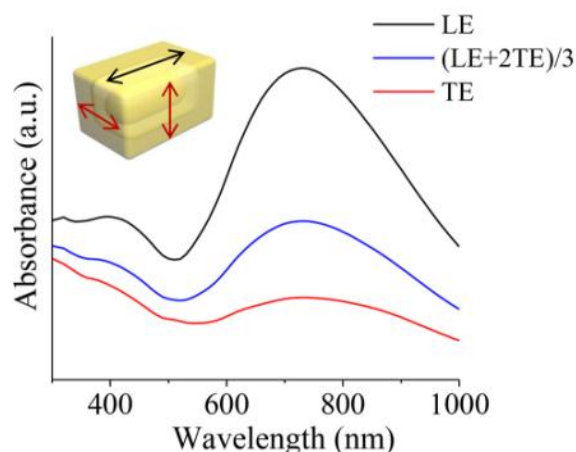


Fig. S12. Calculated absorbance spectra for a single intact CGNR (without any pinholes or rupturing) in aqueous solution ( $n_m = 1.33$ ) along LE (longitudinal edge) and TE (transverse edge) orientation of incident light polarization. Custom generated shape files were used to define the geometry of the target and inter-dipole spacing  $d$  was considered to be 1nm. CGNR was designed as a hollow Au cuboid with an Au NR inside, AuNR was modeled as a cylinder with hemispherical caps at ends. The effect of unpolarized light used in the experiment was incorporated by carrying out two sets of calculations for the structure. Linearly polarized light with polarization along the length [i.e. LE] and width (or height) [i.e. TE] axes was used in calculating the absorbance of a randomly orientated nanocuboid, and the results were averaged with weights of 1/3 and 2/3 respectively, in order to be able to estimate absorbance of the structure under unpolarized radiation. We used the bulk dielectric permittivity values<sup>8</sup> for AuNR, which closely reproduces the experimental absorption spectra. However, the bulk Au permittivity model failed to describe the behavior of thin Au wall of the nanocage (typically few nm) as it does not take into account the increased scattering losses by the electrons. Size dependent correction to Au permittivity model<sup>9</sup> was incorporated to reproduce the characteristics of thin Au walls of the caged-Au NR (CGNR), where the wall thickness was about few nanometers.

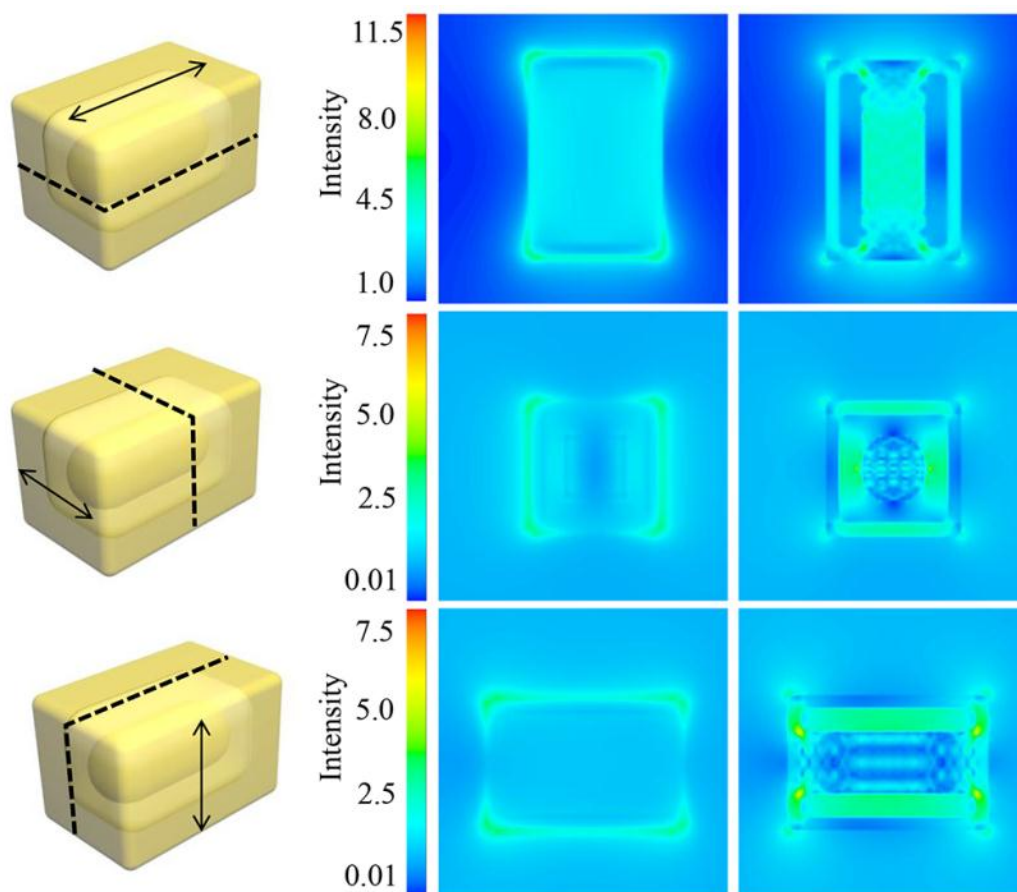













Fig. S13. Near-field calculation of incident light E-field intensity using DDSCAT to evaluate E-field distribution of a single intact CGNR when incident light is polarized along the length (LE), width (TE), and height (TE) axis of the CGNR. Left panel shows the E-field distribution on the outer surface of the CGNR while the right panel depicts the E-field enhancement in the center of the nanobox in three orientations. The E-field distribution indicated that the resonance peaks for both cases, TE and LE in Figure S12, correspond to dipolar resonance modes. Moreover, the intensity of the E-field in each case also depicted the relative difference in the absorption peaks seen for LE and TE orientations.

**TABLE S1.** Proposed morphological models of nanocuboids describing structural evolution during the galvanic replacement reaction process

Structure	L (nm)	W (nm)	Features
 Sample-0	50	36	AuNR@AgNC with rounded edges and corners. This is used as the sacrificial template for the galvanic replacement reaction.
 Sample-1	50	36	The galvanic replacement reaction starts from corners and edges of the nanocuboid in Sample-0. <sup>4</sup> Au is replacing Ag and getting deposited on the surface of nanocuboid. Very thin (~1nm) Au layer deposited on edges and corners making them sharp.
 Sample-2	50	36	More Au deposition (~2nm) on surface, leading to sharper edges and corners of Sample-1. More Au deposition means more Ag is getting dissolved from inside which indicates formation of hollow spaces in nanocuboid interior. Increase in volume is incorporated in effective size parameter.
 Sample-3	52	36	Au completely covers Sample-2 from both ends; the amount of Ag coating on NR has reduced from ends (inside the nanocuboid).
 Sample-4	52	35	More Au is deposited on the surfaces of Sample-3 from ends and sides; amount of Ag coating on NR has reduced from sides as well (inside the nanocuboid). The negative curvature seen on nanocuboid walls are taken into account by slight reduction in width. <sup>4</sup>
 Sample-5	54	36	Uniform cage (2nm wall thickness) is formed, connectors support the NR from both ends, hollow space is modeled to appear around all corners.
 Sample-6	56	38	Cage with 3nm wall thickness, more hollow space and less Ag inside the structure as compared to Sample-5.
 Sample-7	56	38	Ag gets further dissolved, increased hollow space and reduced Ag in cage as compared to Sample-6.
 Sample-8	56	38	More hollow space and less Ag as compared to Sample-7, almost all of the Ag got dissolved in the solution.
 Sample-9	58	38	Cage with wall thickness of ~4nm, Au connectors on ends for NR, no Ag left. The structure has a NR inside cage.
 Sample-10	58	38	Sample-9 broken from two diagonal corners.



Sample-11

58

38

Sample-10 broken further from corners.



Sample-12

58

38

Sample-11 broken further with wall thickness of ~2nm, NR is exposed from one half of the cage.

**TABLE S2.** Structural specifications of intact CGNR models used for simulation of size-tunability

in Fig. 3.

Sample	$L_{\text{CGNR}}$ (nm)	$W_{\text{CGNR}}$ (nm)	$L_{\text{NR}}$ (nm)	$W_{\text{NR}}$ (nm)	$T_{\text{NC}}$ (nm)
Length-1	58	36	46	20	6
Length-2	50	36	40	20	5
Length-3	42	36	34	20	4
Width-1	60	40	46	20	6
Width-2	60	38	46	20	5
Width-3	60	36	46	20	4
Width-4	60	34	46	20	3

**TABLE S3.** Structural Parameters of CGNRs Used in Simulating Cage-Wall-Thickness Effects in Surface Plasmonic Resonances

	Sample	$L_{\text{CGNR}}$ (nm)	$W_{\text{CGNR}}$ (nm)	$L_{\text{NR}}$ (nm)	$W_{\text{NR}}$ (nm)	$T_{\text{NC}}$ (nm)
Figure 4d	Black line	60	38	46	20	5
	Red line	60	40	46	20	5
	Blue line	58	40	46	20	5
Figure 4e	Black line	60	40	46	20	6
	Red line	60	40	46	20	5
	Blue line	60	40	46	20	4



#### Section 4 References

1. (a) N. R. Jana, L. Gearheart and C. J. Murphy, *Adv. Mater.*, 2001, **13**, 1389-1393; (b) B. Nikoobakht and M. A. El-Sayed, *Chem. Mat.*, 2003, **15**, 1957-1962.
2. R. Jiang, H. Chen, L. Shao, Q. Li and J. Wang, *Adv. Mater.*, 2012, **24**, 200-207.
3. Y. Okuno, K. Nishioka, A. Kiya, N. Nakashima, A. Ishibashi and Y. Niidome, *Nanoscale*, 2010, **2**, 1489-1493.
4. (a) X. Lu, J. Chen, S. E. Skrabalak and Y. Xia, *Proceedings of the IMechE, Part N: J. Nanoeng. Nanosyst.*, 2007, **221**, 1-16; (b) E. González, J. Arbiol, V. F. Puntes, *Science*, 2011, **334**, 1377-1380.
5. B. T. Draine and P. J. Flatau, "User Guide for the Discrete Dipole Approximation Code DDSCAT 7.2", 2012, <http://arxiv.org/abs/1202.3424>.
6. B. T. Draine and P. J. Flatau, *J. Opt. Soc. Am. A*, 1994, **11**, 1491-1499.
7. J. Parsons, C. P. Burrows, J. R. Sambles and W. L. Barnes, *Journal of Modern Optics*, 2010, **57**, 356-365.
8. P. B. Johnson and R. W. Christy, *Phys. Rev. B*, 1972, **6**, 4370-4379.
9. D. Sikdar, I. D. Rukhlenko, W. Cheng and M. Premaratne, *Biomed. Opt. Express*, 2013, **4**, 15-31.